THESIS

SUPERHYDROPHOBIC COATINGS FOR ELECTRICAL INSULATORS

Submitted by

Sravanthi Vallabhuneni

Department of Mechanical Engineering

In partial fulfillment of the requirements

For the Degree of Master of Science

Colorado State University

Fort Collins, Colorado

Spring 2018

Master's Committee:

Advisor: Arun K. Kota

Ketul Popat
Matt J. Kipper

ABSTRACT

SUPERHYDROPHOBIC COATINGS FOR ELECTRICAL INSULATORS

Dielectric breakdown in electrical insulators is a frequently encountered phenomenon leading to surface damage, material loss and eventually a complete breakdown of electrical insulators. Dielectric breakdown is accelerated under severe conditions such as humidity and rain. As a result, the service life of the electrical insulators is affected. In our work, we employed superhydrophobic coatings, which are extremely repellent towards water, in an attempt to retain the dielectric strength of electric insulators in the presence of water. In addition, we studied the influence of surface roughness on the dielectric breakdown of electrical insulators.

In this work, hydrophobic PDMS sheets (as a mimic to silicone bushings/insulators) with different surface roughness were fabricated and superhydrophobicity was imparted to these sheets via surface modification. The dielectric breakdown of these PDMS sheets was studied under both dry and wet conditions. The influence of surface roughness on the dielectric breakdown was also investigated by using PDMS sheets with different surface roughness. We noticed an increase in surface roughness leads to lower dielectric breakdown. Further, we demonstrated that superhydrophobic coatings on the surface of electrical insulators allow the retention of dielectric strength under wet conditions. Consequently, we envision that superhydrophobic coatings on electrical insulators will lead to enhanced performance and prolonged service life of insulators.

ACKNOWLEDGEMENTS

I would like to express my special thanks and gratitude to my advisor, Dr. Arun Kota who has constantly encouraged and kept me motivated to finish my work for my thesis in this vast field of surface science. I would like to thank and appreciate Sanli Movafaghi for all the help that she has done with Scanning Electron Microscopy (SEM), Optical Profilometry and for all her wonderful suggestions which helped me to successfully finish this work. I would like to thank all the students in Dr. Kota's research group, Hamed Vahabi, Wei Wang, Lewis Boyd, Anudeep Pendurthi, Matt Cackovic and Dan Sutherland for maintaining an active environment in the lab and for being engaged in the prolonged discussions about my research in the research group meetings. I Sincerely, thank Dr. Matt J Kipper and Dr. Ketul Popat for giving me their valuable time and for their efforts in providing me their feedback to make this work better. I also thank the Office of Naval Research for funding this work through STTR grant.

TABLE OF CONTENTS

1. INTRODUCTION

Dielectric materials are used for a wide variety of applications like indoor insulators, bushings, high voltage and low voltage insulators, surge arrestors, cable terminations, insulation coatings etc.[1–4] Porcelain, epoxy resins, silicone rubber and oil-impregnated paper are well known for their applications as dielectric insulators and there has been a constant interest in the advancing technology of manufacturing to a better grade of dielectric materials.[1–10]

Insulating materials can withstand a certain electric field without losing their insulating properties under an applied voltage. When an insulator undergoes dielectric breakdown, then it permits the passage of electric current.[11–16] Typically this phenomenon is encountered in electrical insulators under high voltage conditions that lead to the material damage.[17] Consequently, the material loses its insulation properties. However, under severe conditions like humidity and rain, the dielectric breakdown is significantly accelerated.[18]

The maximum electric field that an insulating material can withstand is termed as the dielectric strength of that material.[19–21] Dielectric strength is measured by applying an increasing voltage over an insulator until the material starts conducting electric current.[17,22–24] The voltage at which an insulator starts to conduct the electric current is referred as the breakdown voltage.[25–29]

Surface roughness, humidity and rain lead to the lower dielectric breakdown,[26,27,30,31] and an early insulator material deterioration. Such conditions impact the longevity of insulator service life and increase the maintenance costs. In this work, we have attempted to resolve the breakdown of electrical insulators under wet conditions using superhydrophobic coatings. Taking advantage of the extreme repellency of superhydrophobic surfaces to water, we employed superhydrophobic coatings on the surface of polydimethylsiloxane (PDMS) sheets (a mimic of silicone

bushings/insulators) to improve the dielectric strength of the electrical insulators under wet conditions. We explained the fundamentals of the surface wettability and the design criteria of superhydrophobic coatings in chapter 2.

The fabrication of hydrophobic and superhydrophobic PDMS sheets, the influence of superhydrophobicity and surface roughness on the dielectric strength of PDMS in dry and wet conditions are explained in chapter 3.

The conclusions and the future scope of our work is presented in chapter 4.

2. SURFACE WETTABILITY AND SUPERHYDROPHOBICITY

Surface wettability governs how much a liquid wets and spreads on a solid surface and is typically characterized using contact angle and contact angle hysteresis. In nature, biological surfaces like lotus leaf, desert beetles, pitcher plants, shark skin exhibit a surface wettability different from each other, which serve a specific purpose in their life cycle.[32,33] Recently, researchers have been keenly working on exploring the different aspects of surface wettability and the fabrication[34,35,36,37] of such surfaces in order to leverage the advantages of surfaces with special wettability in the applications like anti-fouling, heat transfer, dew collection, surface drag reduction and anti-icing.[33,38–42,37,43] The fundamentals of surface wettability along with the design criteria of superhydrophobic surfaces which are extremely repellent towards water will be discussed in chapter 2. In our work, we utilized these fundamental concepts, for the fabrication of PDMS sheets with different surface wettability.

2.1 Contact Angle (θ) and Contact Angle Hysteresis ($\Delta\theta$)

Contact angle is defined as an angle made by the liquid droplet contacting a solid surface between the tangents of the liquid–vapor and solid–liquid interfaces when measured through the liquid (see Figure 1).[33,44] If the solid surface is non-textured and non-reactive, then the contact angle made by the liquid droplet is termed as the equilibrium contact angle. The equilibrium contact angle on a non-textured and non-reacting surface is given by Young's relation as:[45]

$$\cos(\theta_Y) = \frac{\gamma_{SV} - \gamma_{SL}}{\gamma_{LV}} \tag{1}$$

where γ_{SV} is the solid surface energy, γ_{SL} is the solid – liquid interfacial energy and γ_{LV} is the liquid surface tension. This equation can be thought of as a force balance on a liquid droplet in the equilibrium state. As indicated by the equation 1, on a given surface, high surface tension liquids

exhibit higher contact angles. In the same way, for a specific test liquid, surfaces with low solid surface energy display higher contact angles. Therefore, for the fabrication of surfaces that display higher contact angles with a specific liquid, materials with low solid surface energy are preferred. A surface is classified as hydrophobic, if it displays contact angles that are greater than 90° with water and as hydrophilic if the contact angles are less than 90°with water.

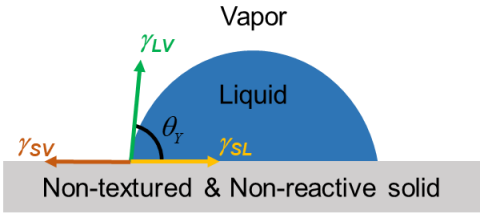

Figure 1: Schematic illustrating the force balance on a liquid droplet in contact with a non-textured and non-reactive surface.

The contact angle hysteresis is another important parameter of surface wettability that is defined as the difference between the advancing (the maximum) and the receding (the minimum) contact angles of a liquid droplet on a given surface.[44,46] The physical (i.e. surface texture) and chemical (i.e. surface energy) inhomogeneities on the surface give rise to contact angle hysteresis ($\Delta\theta$).[32,33,47] Physically, the contact angle hysteresis reflects the energy dissipated in the motion of a liquid droplet on a solid surface. A low contact angle hysteresis on a given surface indicates a low adhesion between the liquid and the solid. Hence, the lower the contact angle hysteresis, the higher is the mobility of liquid droplets on a surface.

2.2 Roll-off/Sliding angle

The minimum tilt angle of a solid surface relative to horizontal at which a liquid droplet starts to slide or roll-off from the surface is defined as roll-off/sliding angle (see Figure 2). The roll-off or sliding angle is given by Furmidge relation as:[48]

$$\sin(\omega) = \frac{\gamma_{LV} w(\cos\theta_R - \cos\theta_A)}{\rho g V} \qquad (2)$$

where ω is the roll-off/sliding angle, γ_{LV} is the surface tension of a liquid, w is the width of the droplet at triple phase contact line perpendicular to its motion, θ_R is the receding contact angle, θ_A is the advancing contact angle, ρ is the density of liquid, g is the acceleration due to gravity and V is the volume of the droplet. This equation is derived by doing an energy balance on a droplet that is sliding on a surface under gravity with the assumptions – i) The solid surface is physically and chemically homogeneous. ii) The shape of the droplet at triple phase contact line is rectangle.

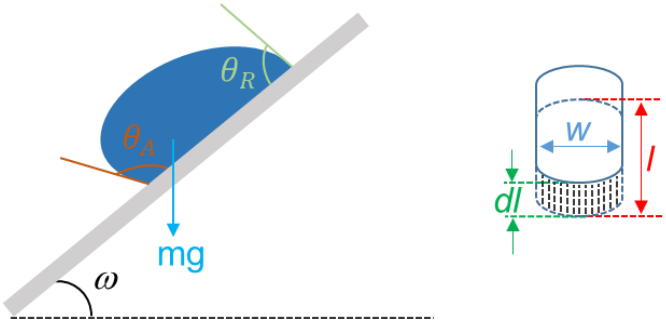

Figure 2. Schematic of a liquid droplet sliding on a smooth surface tilted at an angle ω *relative to the horizontal.*

2.3 Textured Surfaces

When a liquid droplet contacts a textured surface, it displays an apparent contact angle (θ^*) on the macroscale, which is different from the Young's contact angle that is displayed on non-textured surfaces. In this case, it can adopt one of the two thermodynamic states to minimize overall free energy – the Wenzel state or the Cassie-Baxter state. In the Wenzel state, the liquid forms a homogeneous liquid-solid interface and consequently, fully wets the surface (see Figure 3). The surface roughness was characterized by Wenzel using the roughness factor (r) as:[49]

$$Roughness\ factor\ (r) = \frac{Actual\ Surface\ Area}{Projected\ Surface\ Area} \tag{3}$$

The roughness factor (r) for any surface is always greater than one. The apparent contact angle (θ_W^*) of a droplet in Wenzel state can be determined using the equation 4.[49]

$$\cos(\theta_W^*) = r\cos(\theta_Y) \tag{4}$$

where r is the roughness factor and θ_Y is the Young's contact angle. It is evident from the equation 4, that with an increase in the roughness factor, a surface displays $\theta_W^* << 90^0$ if it has $\theta_Y < 90^0$ and $\theta_W^* >> 90^0$ if it has $\theta_Y > 90^0$.

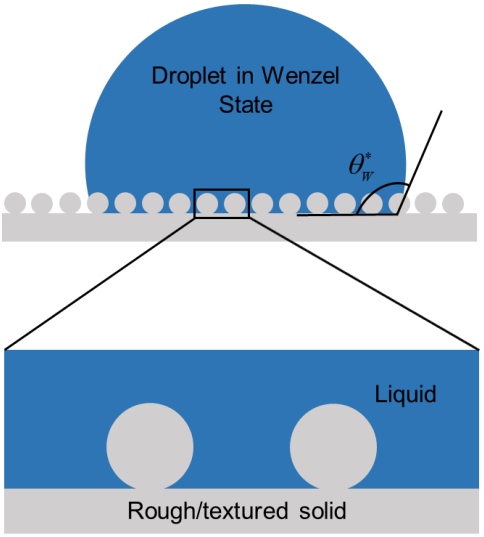

Figure 3. Schematic of a liquid droplet in Wenzel State on a textured surface.

In the Cassie-Baxter state, the liquid droplet wets the solid surface partially by trapping air pockets in between the solid surface features underneath the droplet. Hence, a composite interface of solid-liquid-air is formed between the solid surface and the liquid droplet (see Figure 4). The apparent contact angle (θ_{CB}^*) of a liquid droplet in this state can be determined using the relation given by Cassie and Baxter as[50]:

$$\cos(\theta^*) = f_{SL}\cos(\theta_Y) + f_{LV}\cos(\pi) \tag{5}$$

where f_{SL} is the area fraction of solid and liquid interface and f_{LV} is the area fraction of liquid and vapor interface. As indicated by the equation 5, the apparent contact angle is the function of area fractions of solid-liquid and liquid vapor interfaces. An increase in liquid-vapor area fraction displays higher contact angles and leads to low contact angle hysteresis. Cassie-Baxter state is a preferred state for designing superhydrophobic (extremely repellent to water) surfaces.

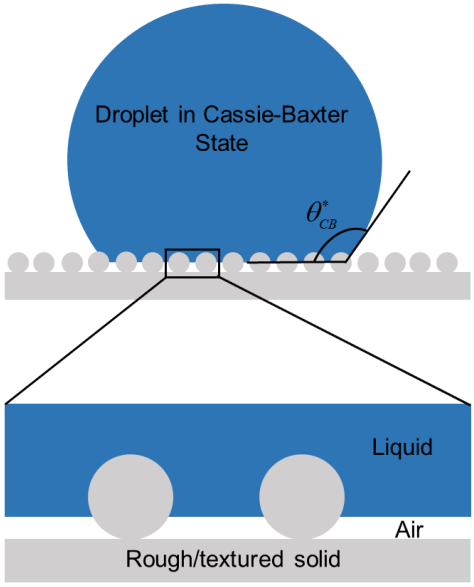

Figure 4. Schematic of a liquid droplet in Cassie-Baxter State on a textured surface.

2.4 Hierarchical Structure

Hierarchical structure is referred as the surface texture where the coarser length scale features are covered with the features of finer length scales (see Figure 5). If the hierarchical structure supports Cassi-Baxter state, then this type of structure traps the air pockets both on coarser and finer length scale features. Thereby, the effective liquid-vapor area fraction increases significantly leading to higher apparent contact angles and lower contact angle hysteresis. The advantage of a hierarchical structure is that it increases the surface roughness along with an increase in liquid-vapor area fraction rendering the surface more hydrophobic.[51]

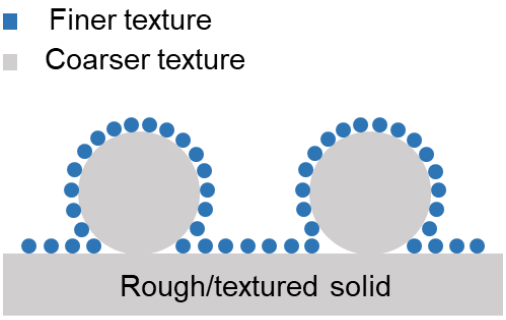

Figure 5. Schematic representing the hierarchical structure on a textured solid.

2.5 Fabrication of Superhydrophobic Surfaces

On superhydrophobic surfaces, water droplets display contact angles that are greater than 150° (θ^* >150°) and $\Delta\theta$ <10°. Superhydrophobic surfaces are fabricated by reducing the solid surface energy using low-energy materials like fluorinated silica particles and by introducing the appropriate (e.g. macroscale/nanoscale) structure.[37] In our work, we imparted low solid surface energy by treating the surface with a fluorinated silane and introduced the hierarchical texture by spray coating silica particles over the surface in order to fabricate superhydrophobic surfaces. The fabrication process is discussed in detail in chapter 3.

3. SUPERHYDROPHOBIC COATINGS FOR ELECTRICAL INSULATORS

3.1 Background

Dielectric breakdown is a common problem encountered in various electrical apparatus (e.g., power transformers, circuit breakers, power capacitors, etc.). It occurs in insulators when a voltage exceeding the breakdown voltage is applied across the material.[19–21] This problem arises due to the drastic reduction in dielectric strength (i.e., the resistance of the material to the passage of electric current) and is always accompanied by material deterioration. The dielectric strength is approximated as the electric field at the breakdown voltage and is given as[52,53]:

$$E_d = \frac{V_{bd}}{t} \tag{6}$$

where E_d is the dielectric strength of an insulator, V_{bd} is the breakdown voltage, and t is the thickness of the insulator over which the electric field is applied.

Dielectric strength can be affected by a few external factors like surface roughness, electrode geometry and material impurities.[26,27] Under dry conditions (i.e. absence of water), as the electric field applied across a dielectric material increases, there will be an onset of corona discharge due to leakage currents. The corona discharge results in a surface damage of an insulator.[54–56] This surface damage propagates through the material, layer by layer causing a considerable material loss and expediting the aging of the material.[57] If the applied voltage is further increased, the corona discharge is amplified and an electric arc is developed. The electric arc is a major source of heat and causes a thermal breakdown of the material resulting in a significant material loss followed by dielectric breakdown.

In wet conditions, humidity and water play a key role in affecting the dielectric strength of a material.[30,31] In the presence of water or moisture, as the electric field is applied across dielectric

materials, surface damage occurs due to the intensification of electric field on water.[58] Since there are high electric fields distributed in the water at low voltages, the dielectric breakdown occurs at low voltages.[55,59] Further, the presence of water gives rise to high leakage currents as the permittivity of water is 80 times higher than air.[60] Consequently, there would be an earlier onset of corona at the electrode. As leakage currents due to corona discharge amplify, the electric arc occurs at lower voltages. This electric arc leads to thermal breakdown of the dielectric material at lower voltages.[25,61,59,62] This thermal breakdown leads to material deterioration and loss, which in turn result in electrical breakdown.[63] Consequently, the service life of an insulator is affected. For example, in real scenarios, wet conditions like rain or humidity rapidly reduce the life of high voltage bushings by reducing the dielectric strength. When these bushings fail, they must be replaced with the new ones. Consequently, there will be an increase in maintenance cost. Further, the productivity of power transformers will be reduced due to the downtime during repair.[64] Therefore, fabrication of insulators that minimize the interaction with water is paramount to reduce the risk of failure, provide lower life and reduce the operating costs of insulators.

In this work, we have attempted to resolve the breakdown of electrical insulators under wet conditions using superhydrophobic coatings. Taking advantage of the extreme repellency of superhydrophobic surfaces to water, we employed superhydrophobic coatings on the surface of polydimethylsiloxane (PDMS) sheets (a mimic of silicone bushings/insulators) to improve the dielectric strength of the electrical insulators under wet conditions. We chose to use PDMS because it is commercially available and can be easily casted into sheets. We investigated the influence of surface wettability on the dielectric strength of insulator materials under dry and wet conditions. In addition, the effect of surface roughness (which is required for superhydrophobic surfaces) on

dielectric strength is studied. We envision that developing insulators that retain their dielectric strength under wet conditions will improve their service life.

3.2 Materials and Methods of Fabrication

3.2.1 Materials/Equipment

Sand papers of 120 and 60 grit sizes were ordered from Johnson abrasives and commercially available two-part Sylgard 184 Silicone elastomer base and its cross-linker was purchased from Dow Corning. Heptadecafluoro tetrahydrodecyl trichlorosilane was ordered from Gelest. Degassing and curing of the PDMS was done using the vacuum oven (Across International). Plasma etcher (Plasma etch) was used to treat PDMS sheets with oxygen plasma. The sample thickness was measured with the optical microscope (Amscope FMA050). The optical profilometry and scanning electron microscope was used to characterize surface morphology and measure surface roughness (R_{rms}), respectively. The contact angles and roll-off angles were measured using the contact angle goniometer (Ramé-Hart 260F4 goniometer).

3.2.2 Fabrication of uncoated PDMS sheets

Uncoated PDMS sheets were fabricated using Sylgard 184 Silicone elastomer base and its cross-linker. The silicone elastomer base and cross-linker were added in 10:1 ratio in a paper cup and were stirred vigorously until they are thoroughly mixed. Later, the solution was degassed using a vacuum oven until there were no more air bubbles trapped within the transparent solution. For our work, we needed PDMS sheets with low enough thickness so that the PDMS sheets can breakdown at voltages less than 30 kV (limit of the power supply). We controlled the thickness of the sheets by varying the mass of PDMS solution used for casting.

In order to fabricate smooth/non-textured PDMS sheets, 3 grams of PDMS solution was poured into a polystyrene petri dish. This petri dish was placed on a digital weighing scale. As soon as the

solution was added to a petri dish, it conformed to the shape of petri dish. Since the petri dish surface was smooth, the cured PDMS sheets were also smooth/non-textured. While PDMS could be cured for 24 hours at room temperature, in order to expedite the curing process, we cured PDMS by placing it in an oven at 70°C for 90 minutes. Once cured, PDMS should be solid and transparent, devoid of any air bubbles. This transparent PDMS was peeled off gently from the surface along the circumference of the petri dish to avoid any tears in the sheet in the process.

Rough PDMS sheets were fabricated by casting PDMS on 120 (smoother) and 60 (rougher) grit size sand papers, which are denoted as 120G and 60G sand/abrasive papers in this work. The conformity of liquid PDMS on abrasive particles of varying sizes imparted different surface roughness to the sheets. In order to prepare rough PDMS sheets, the 120G and 60G sand paper were cut into 4 cm x 4 cm samples. These sand papers were then silanized with heptadecafluoro tetrahydrodecyl trichlorosilane silane to impart low solid surface energy (see Figure 6a). By imparting the low surface energy to the sand papers, the PDMS could be peeled off without tearing. The sand papers were treated with 125 µl silane via vapor phase silanization[65,66] in a closed chamber (inverted glass bowl) at 120°C for one hour (see Figure 6f). This surface modification renders hydrophobicity to the sand papers. The hydrophobic sand papers were then attached to the bottom surface of the petri dish using a double-sided tape. Then, 3.5 grams and 5 grams of PDMS solution were added to the 120G and 60G modified sand papers, respectively (see Figure 6b). The liquid PDMS conformed to the features of the abrasive particles present on the sand paper and spread uniformly over the surface. While the PDMS spreads itself over the surface, there could be some air trapped between the rough features of sand paper and the PDMS. These air bubbles were removed by degassing in the vacuum oven. Subsequently, the PDMS was cured in a vacuum oven at 70°C for 90 minutes. Then, the PDMS was peeled off gently and carefully from the sand papers

(see Figure 6c). Post peeling, these 120G PDMS sheets were anticipated to have lower roughness compared to 60G sand papers. Thus, PDMS sheets with varying surface roughness were fabricated using sand papers (see Figure 6d).

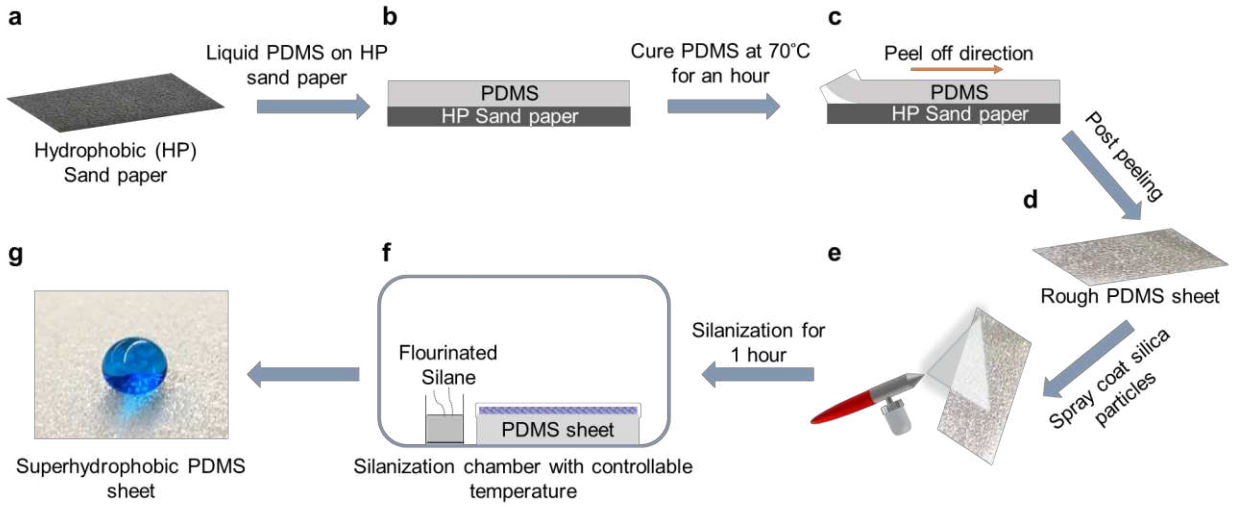

Figure 6. Schematic illustrating the fabrication process of superhydrophobic PDMS sheets using a hydrophobic sand paper.

3.2.3 Fabrication of superhydrophobic PDMS sheets

As discussed in the second chapter, the primary measure of wetting of a liquid on a nontextured (i.e., smooth) solid surface is the equilibrium (or Young's) contact angle θ. When the liquid droplet contacts a textured (i.e., rough) solid surface, it displays an apparent contact angle θ^*, and it can adopt one of the following two configurations to minimize its overall free energy: the fully wetted Wenzel state or the Cassie−Baxter state. The Cassie−Baxter state is preferred for designing super-repellent surfaces because it leads to high θ^* and low CAH. Any surface, to exhibit superhydrophobicity should possess low solid surface energy along with appropriate (e.g., microscale or nanoscale) texture. Introducing the appropriate texture on the surface enables water

droplets to adopt a robust Cassie-Baxter state and display high apparent contact angles (θ^*) and low contact angle hysteresis ($\Delta\theta^*$).

To fabricate the superhydrophobic PDMS sheets, the uncoated (smooth/non-textured) PDMS sheets prepared in section 3.2.2 were first spray coated with silica particles (see Figure 6e). A spray coating solution was prepared by mixing 20 ml hexane with 400 mg of 7 nm silica particles. This solution was spray coated uniformly over non-textured and textured hydrophobic PDMS sheets using a spray coater. The spray coating was performed maintaining a distance of 30 cm between the spray coater and the sample in order to ensure that the hexane mostly evaporated during the process. This was done in order to prevent swelling of PDMS by hexane. Then, the spray coated PDMS sheets were dried for 2 minutes and placed in the plasma chamber. Oxygen plasma treatment forms hydroxyl groups over the surface which reacts readily with silane. So, oxygen plasma treatment was conducted for 15 minutes. After plasma treatment, these sheets were treated with 200 µl silane via vapor phase silanization in a closed chamber (inverted glass bowl) at 120°C for 45 minutes (see Figure 6f). This surface modification imparts low solid surface energy and renders superhydrophobicity to the PDMS sheets.[67] After this process, PDMS sheets displayed superhydrophobicity with apparent contact angles (θ^*) greater than 150° and low roll-off angles (see Figure 6g). In this work, the smooth, 120G and 60G PDMS sheets which were spray coated with SiO_2 and treated with fluorinated silane are referred as F-SiO_2 on smooth, F-SiO_2 on 120G and F-SiO_2 on 60G respectively.

3.2.4 Thickness Measurements

The thickness of the PDMS sheets along the cross-section was measured using an optical microscope and a 10X objective was used. The samples were imaged and analyzed using Amscope

software. A minimum of five measurements per sample were taken and the error of thickness was $\pm$0.008 mm.

3.2.5 Scanning Electron Microscopy

The surface morphology of the samples was imaged using scanning electron microscopy (SEM) (JEOL JSM-6500F) at 15 kV.

3.2.6 Optical Profilometry

All surface roughness measurements were conducted using an optical profilometer (Zygo Zescope). Standard deviation was determined based on at least three measurements for each surface.

3.2.7 Contact Angle Goniometry

We characterized the wettability of the PDMS sheets by performing contact angle goniometry with Ramé-Hart 260F4 goniometer. The contact angles were measured by advancing and receding 5 µl droplet on the surface. The roll-off angles were measured by tilting the stage until a 10 µl droplet rolled off from the surface. The error in contact angles and roll-off angles were $\pm 2^{\circ}$ and $\pm 1^{\circ}$, respectively.

3.3 Experimental Set-up for Breakdown Voltage Measurements

3.3.1 Tests in Dry Condition

For all coated and uncoated PDMS sheets, we conducted dielectric breakdown experiments in both dry and wet conditions. As mentioned in chapter 1, the dielectric strength can be affected by temperature as well as size and shape of the electrodes. To ensure the consistency, all the experiments were conducted at room temperatures and spherical copper electrodes with 3 mm diameter were used.

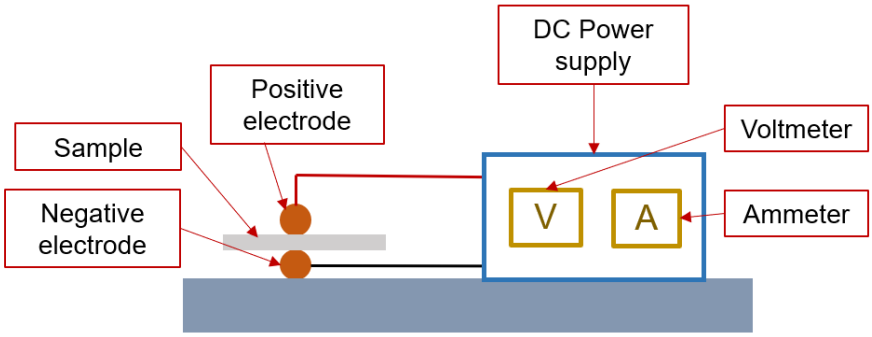

Figure 7. Schematic of the dielectric strength test set up under dry conditions.

A schematic of the test set-up for dry condition is shown in Figure 7. In this set-up, the copper spheres were soldered to the tips of insulated copper wires and were used as positive and negative electrodes. Two electrodes were placed on the top surface and the bottom surface in a way that they contact the surface of the test sample without any gap between them. A DC power supply with 200 μA ammeter and 30 kV voltmeter were used to apply an electric field across the test sample. The whole set up, except the DC power supply along with voltmeter and ammeter, was enclosed in a glass chamber as a safety precaution. The electric field applied across the test samples was controlled using voltmeter manually while conducting the experiments.

An increasing voltage was applied gradually over the sample and the set-up was carefully monitored for any corona discharge or flash overs. The voltage was increased until the electric current passed through the sample. The voltage at which electric current passed through the sample was measured as the breakdown voltage (V_{bd}) of the sample. This breakdown voltage was identified as the voltage beyond which, with an increase in voltage, the voltmeter read zero and there was a current generated as per the ammeter readings indicating that there was a flow of current between electrodes and the potential difference between to electrodes is nullified. The dielectric strength (E_d) of PDMS sheets is calculated with the equation 6 by using the values of

the breakdown voltage and the thickness (t) of the sheet. For each PDMS sheet, three measurements were conducted.

3.3.2 Tests in Wet Condition

The dielectric breakdown tests in wet conditions were conducted using a set up similar set-up to that used for dry conditions, but the tests were done in the presence of water droplets. The schematic for the tests in wet condition is shown in the figure 7. The PDMS sheets were placed in between the electrodes and de-ionized water droplets were added uniformly over the surface using a 1 milliliter syringe. Later, an electric field was applied over the PDMS surface and the voltage was gradually increased until it reached a breakdown voltage. For each PDMS sheet, three measurements were conducted.

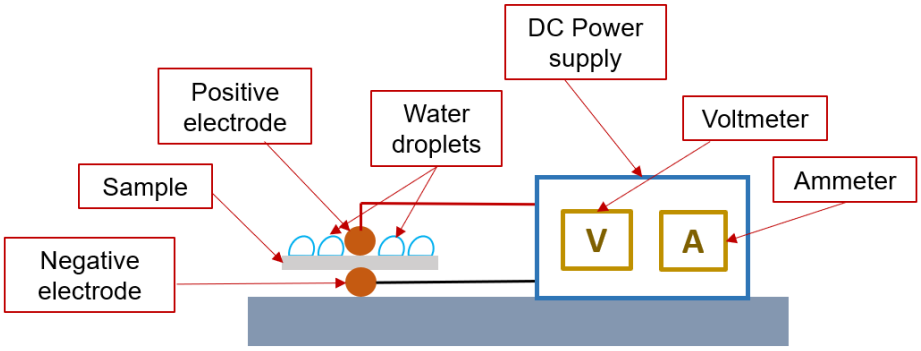

Figure 8. Schematic showing the dielectric strength test set up under wet conditions.

3.4 Results and Discussions

3.4.1 Surface Morphology and Surface Roughness

In this work, scanning electron microscopy (SEM) was conducted to study the surface morphology of the PDMS sheets. Figure 9a, Figure 9b and Figure 9c are the SEM images of uncoated smooth/non-textured, 120G and 60G PDMS sheets, respectively. From the Figure 9a, it is evident that uncoated non-textured surface is relatively smoother and possess lower surface roughness compared to that of other PDMS sheets. The 120G and 60G PDMS sheets displayed

noticeable grooves on the surface in their SEM images and these grooves contribute to an amplified surface roughness.

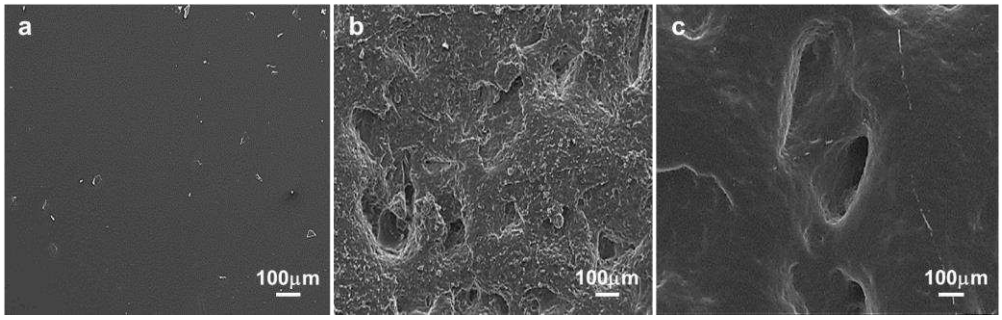

*Figure 9. SEM images of the uncoated PDMS sheets. (**a**-**c**) The SEM images of uncoated non-textured, 120G and 60G PDMS sheets, respectively.*

Figure 10a, Figure 10b and Figure 10c show the SEM images of coated smooth, 120G and 60G PDMS sheets, respectively. The SEM images (Figure 10a, 10b and 10c) indicates that the surface roughness is amplified due to the silica particles and its agglomerates that are spread over the coated PDMS sheet surfaces. This surface texture on the surface imparts a high surface roughness to the coated PDMS sheets. The surface roughness coupled with a low solid surface energy (imparted from silanization) render these coated PDMS sheets superhydrophobic.

Optical profilometry was performed on these PDMS sheets to analyze the surface roughness (R_{rms}). The surface roughness (R_{rms}) of uncoated and coated PDMS sheets is reported in the Table 1. As predicted (from SEM images), the uncoated smooth/non-textured PDMS sheets exhibited the least surface roughness (R_{rms}) and is followed by 120G and 60G PDMS sheets, respectively, in increasing order. The same trend in surface roughness is observed with the coated PDMS sheets (i.e. the coated 60G PDMS sheets have the highest surface roughness and coated non-textured PDMS sheets exhibited the lowest surface roughness (see Table 1).

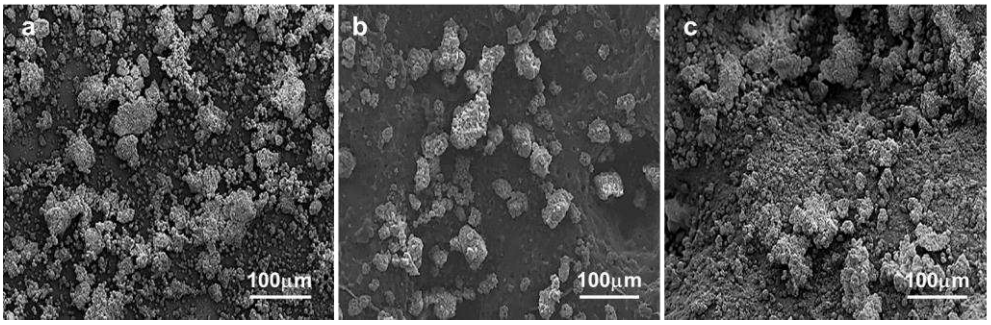

*Figure 10. SEM images of the coated PDMS sheets. (**a**-**c**) The SEM images of coated smooth, 120G and 60G PDMS sheets, respectively.*

Table 1. Surface roughness (R_{rms}) of PDMS sheets from optical profilometry.

Sample	R_{rms} [μm]	
	Uncoated PDMS sheets	Coated PDMS sheets
Smooth/Non-textured	0.05 ± 0.001	5.5 ± 0.73
120G	6.28 ± 0.87	9.86 ± 0.73
60G	8.8 ± 0.69	14.36 ± 0.93

3.4.2 Characterization of Wettability

The surface wettability of our PDMS sheets were characterized using contact angle goniometry. The advancing and receding contact angles of water on uncoated PDMS sheets are listed in the Table 2 and are shown in the Figure 11 (left). All the uncoated PDMS sheets displayed the advancing contact angles greater than 120° and a high $\Delta\theta^*$. The water droplets did not slide past the surface of these PDMS sheets even at a tilt angle of 90°. It implies that the water droplets were in Wenzel state on uncoated 120G and 60G PDMS surfaces leading to a high contact angle hysteresis on the surface. On the contrary, the advancing contact angles of water on the coated PDMS sheets (see Figure 11 (right) and Table 2) were close to 150° and $\Delta\theta^*$ is less than 10°. The measured roll-off angles were less than 5° (see Table 3). The roll-off angles were predicted based

on the Furmidge relation (see section 2.2), which is derived by balancing the work done by gravity on a liquid droplet with the work done by adhesion of the droplet. The width of the droplet (w) is calculated by the following equation with an assumption that the shape of the droplet resembles a spherical cap.[68]

$$w = 2\cos(\bar{\theta}^* - \frac{\pi}{2})[\frac{3V}{\pi(2-3\cos\bar{\theta}^* + \cos^3\bar{\theta}^*)}]^{\frac{1}{3}} \quad (7)$$

Where $\bar{\theta}^*$ is the average apparent contact angle, given as:

$$\cos\bar{\theta}^* = \frac{\cos\theta^*_{adv} + \cos\theta^*_{rec}}{2} \quad (8)$$

The predicted values matched reasonably well with the measured values with an error less than 3°. The slight difference between the measured and the predicted values can be attributed to the non-uniformly aligned surface features over PDMS sheets, chemical inhomogeneities on the surface, the error from the contact angle measurements and the assumptions in the Furmidge equation.

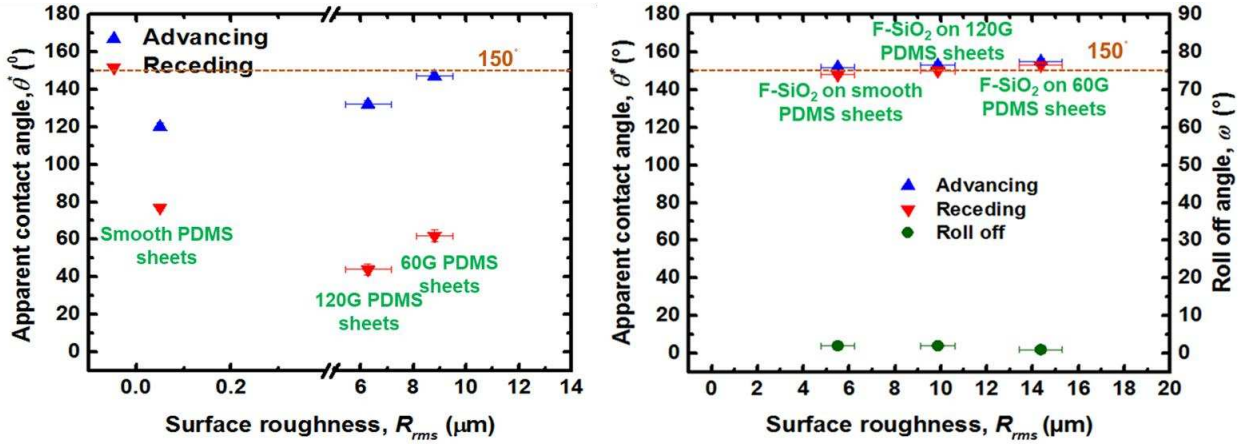

Figure 11. The advancing and receding contact angles of uncoated PDMS sheets (left), the advancing contact angles, receding contact angles and the roll-off angles of coated PDMS sheets (right).

Table 2. The advancing, receding contact angles of uncoated and coated PDMS sheets.

Sample	Uncoated PDMS sheets		F-SiO_2 on PDMS sheets	
	θ_A^* [°]	θ_R^*[°]	θ_A^* [°]	θ_R^*[°]
Smooth/Non-textured	120	77	152	148
120G	132	44	153	150
60G	147	62	155	153

Table 3. The predicted and measured roll-off (ω) angles of coated PDMS sheets.

Sample	F-SiO_2 on PDMS sheets	
	ω (measured) [°]	ω (predicted) [°]
Smooth/Non-textured	2	1.3
120G	2	0.9
60G	1	0.5

3.4.3 Dielectric Strength Measurements

3.4.3.1 Uncoated PDMS – Dielectric Strength under Dry vs. Wet Conditions

The dielectric strength of uncoated PDMS sheets was calculated using equation 6 and listed in the Table 4 and shown in Figure 12 (left). The results indicate that all the PDMS sheets have exhibited higher dielectric strength in dry conditions compared to wet conditions. The PDMS sheets have displayed a considerable drop in their dielectric strengths in wet conditions (see Table 6). This is because the electric permeability of water is 80 times higher than that of air.[60] In the presence of water (i.e., wet conditions), when an electric field is applied over the surface, the high electric permeability leads to an increase in space charge distribution on water. A high space charge distribution leads to an intensification of the electric field on the water droplet. This intensified electric field results in an earlier breakdown (breakdown at lower voltages) of the PDMS sheets and leads to lower dielectric strength.

Surface roughness is another key factor that influences the dielectric strength of PDMS sheets. We observed that with an increase in surface roughness, there is a drop in the dielectric strength under both dry and wet conditions (see Figure 12). Under an applied voltage, as the surface roughness increases, the surface area that is exposed to the electric field also increases. Consequently, there is a high probability to expose the surface defects to the electric field, leading to an early dielectric breakdown by passing the electric current through the least resistant path of surface defects. In addition, under an electric field, the charges tend to concentrate on the sharp features on a surface.[69] This charge concentration over the sharp features may have also contributed to an accelerated dielectric breakdown.

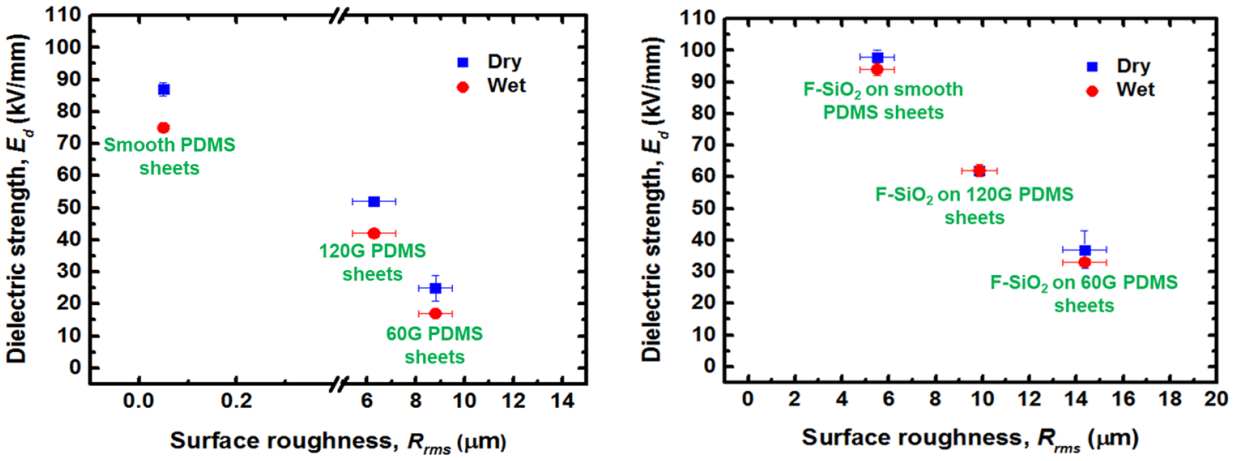

Figure 12. The dielectric strength of uncoated PDMS sheets under dry and wet conditions (left), the dielectric strength of coated PDMS sheets under dry and wet conditions (right).

Table 4. Dielectric strength (E_d) of uncoated PDMS sheets in dry and wet conditions.

Sample	E_d [kV/mm]	
	Dry conditions	Wet conditions
Smooth/Non-textured	87 ± 2	75 ± 1
120G	52 ± 1	42 ± 1
60G	25 ± 4	17 ± 1

3.4.3.2 Coated PDMS – Dielectric Strength under Dry vs. Wet Conditions

The dielectric strengths of coated PDMS sheets under dry and wet conditions are reported in Table 5 and Figure 12 (right). The error reported is the standard deviation obtained from three measurements. Unlike the uncoated PDMS sheets, the coated PDMS sheets did not show a significant drop in dielectric strengths under wet conditions compared to dry conditions. In other words, the dielectric strength of coated PDMS sheets in wet conditions was nearly the same as that in dry conditions. Although the water droplets were stable on coated PDMS sheets when they were placed, they rolled past the surface as soon as the electric field was applied. This is due to the charge acquired by the droplets in the presence of electric field. Because of this acquired charge, the onset of repulsive forces between the droplets with the same charge drove them away from their positions on the surface. The superhydrophobic nature of PDMS sheets aided the droplets to roll off from the surface by virtue of its low contact angle hysteresis. Consequently, the presence of water on superhydrophobic PDMS sheets did not change the dielectric strength of PDMS sheets significantly (see Table 6).

The dielectric strength exhibited of coated PDMS sheets is higher than the uncoated PDMS sheets under dry conditions. This could be attributed to the thin porous layer of silica that is adhered to the surface of coated PDMS sheets. Silica has higher dielectric strength compared to that of PDMS. So, the dielectric strength of coated PDMS sheets is higher than its uncoated counterparts in dry conditions. Similar to that observed with uncoated sheets, the surface roughness has an adverse effect on the dielectric strength. Figure 12 indicates that the dielectric strength of coated PDMS sheets decreases with an increase in surface roughness (refer section 3.4.3.1). Thus, our results suggest that superhydrophobic coatings can prevent the earlier breakdown of electrical insulators under wet conditions and result in a longer service life.

Table 5. Dielectric strength (E_d) of coated PDMS sheets in dry and wet conditions.

Sample	E_d [kV/mm]	
	Dry conditions	Wet conditions
F-SiO_2 on Smooth	98 $\pm$ 2	94 $\pm$ 2
F-SiO_2 on 120G	62 $\pm$ 2	62 $\pm$ 2
F-SiO_2 on 60G	37 $\pm$ 6	33 $\pm$ 1

Table 6. Change in the dielectric strength (ΔE_d) of PDMS sheets in dry and wet conditions.

Sample	E_d [kV/mm]					
	Uncoated PDMS sheets			F-SiO_2 on PDMS sheets		
	Dry	Wet	Change (ΔE_d)	Dry	Wet	Change (ΔE_d)
Smooth	87	75	12	98	94	4
120G	52	42	10	62	62	0
60G	25	17	8	37	33	4

4. CONCLUSIONS AND FUTURE WORK

4.1 Conclusions

In this work, we fabricated PDMS sheets with varied surface roughness and different surface wettability. We have investigated the influence of surface roughness and superhydrophobicity on the dielectric strength of PDMS sheets under both dry and wet conditions. We observed that the dielectric strength of PDMS sheets under wet conditions does not decrease significantly in the presence of superhydrophobic coatings, despite their surface roughness. We anticipate that superhydrophobic coatings will result in a prolonged service life of electrical insulators even in wet conditions like rain.

4.2 Future Work

In this work, we used DC power supply to test all the conditions of dielectric strength because we wanted to test the influence of superhydrophobic coatings on high voltage bushings. Most of the indoor insulation applications typically use AC power supply rather than DC. The study on dielectric breakdown in dry and wet conditions using AC power supply will help in the investigation of this issue in electrical insulators that are used in indoor applications. Further, PDMS particles can be spray coated on the surface of hydrophobic PDMS sheets to fabricate superhydrophobic PDMS sheets instead of silica particles to study the influence of surface roughness on dielectric strength. Through this process, the effect of surface roughness on the dielectric strength can be understood better by comparing the dielectric strength of hydrophobic PDMS sheets with that of superhydrophobic PDMS sheets. This work can also be extended to the different dielectric materials like porcelain, oil-impregnated paper, epoxy resins etc. which are being used as insulators in different applications like cable lines, bushings, etc. In future, this work can be extended to conduct the in-situ experiments mimicking the rain environment on our

superhydrophobic surfaces. Conducting in-situ tests can confirm that these coatings can be used in practical applications in which insulators are exposed to rain. In addition, the durability, which is a major concern with superhydrophobic coatings, must be improved. In severe conditions like extreme rainfall, the rain water can wash the coating off from the surface and make the surface relatively less hydrophobic. Any superhydrophobic coating with high durability can be a replacement to the coating we used and can result in good service life of insulators under adverse conditions like rain.

REFERENCES

1. Hall, J. & Orbeck, T. Evaluation of a New Protective Coating for Porcelain Insulators. *IEEE Trans. Power Appar. Syst.* **PAS-101,** 4689–4696 (1982).

2. Occhini, E. & Maschio, G. Electrical Characteristics of Oil-Impregnated Paper as Insulation for HV DC Cables. *IEEE Trans. Power Appar. Syst.* **PAS-86,** 312–326 (1967).

3. Ehsani, M., Borsi, H., Gockenbach, E., Bakhshandeh, G. R. & Morshedian, J. Modified silicone rubber for use as high voltage outdoor insulators. *Adv. Polym. Technol.* **24,** 51–61 (2005).

4. Hall, J. F. History and bibliography of polymeric insulators for outdoor applications. *IEEE Trans. Power Deliv.* **8,** 376–385 (1993).

5. Lundgaard, L. E., Hansen, W., Linhjell, D. & Painter, T. J. Aging of Oil-Impregnated Paper in Power Transformers. *IEEE Trans. Power Deliv.* **19,** 230–239 (2004).

6. Xingliang Jiang *et al.* Comparison of DC Pollution Flashover Performances of Various Types of Porcelain, Glass, and Composite Insulators. *IEEE Trans. Power Deliv.* **23,** 1183–1190 (2008).

7. Institution of Electrical Engineers., F. V., Gonos, I. F. & Stathopulos, I. A. *IEE proceedings. Generation, transmission, and distribution. IEE Proceedings - Generation, Transmission and Distribution* **148,** (Institution of Electrical Engineers, 1994).

8. Bok-Hee Youn & Chang-Su Huh. Surface degradation of HTV silicone rubber and EPDM

used for outdoor insulators under accelerated ultraviolet weathering condition. *IEEE Trans. Dielectr. Electr. Insul.* **12,** 1015–1024 (2005).

9. Momen, G. & Farzaneh, M. Survey of micro/nano filler use to improve silicone rubber for outdoor insulators. *Rev.Adv.Mater.Sci* **27,** 6–7 (2011).

10. Chisholm, W. A. *et al.* The cold-fog test [for outdoor insulators]. *IEEE Trans. Power Deliv.* **11,** 1874–1880 (1996).

11. Gatti, D. *et al.* The dielectric breakdown limit of silicone dielectric elastomer actuators. *Appl. Phys. Lett.* **104,** 52905 (2014).

12. Tanaka, T. Dielectric nanocomposites with insulating properties. *IEEE Trans. Dielectr. Electr. Insul.* **12,** 914–928 (2005).

13. Takahashi, T., Okamoto, T., Ohki, Y. & Shibata, K. Breakdown strength at the interface between epoxy resin and silicone rubber - A basic study for the development of all solid insulation -. *IEEE Trans. Dielectr. Electr. Insul.* **12,** 719–724 (2005).

14. Blok, J. & LeGrand, D. G. Dielectric Breakdown of Polymer Films. *J. Appl. Phys.* **40,** 288–293 (1969).

15. Kao, K. C. New theory of electrical discharge and breakdown in low-mobility condensed insulators. *J. Appl. Phys.* **55,** 752–755 (1984).

16. Zener, C. A Theory of the Electrical Breakdown of Solid Dielectrics. *Proc. R. Soc. A Math. Phys. Eng. Sci.* **145,** 523–529 (1934).

17. Jongen, R., Morshuis, P., Smit, J., Janssen, A. & Gulski, E. A statistical approach to

processing power transformer failure data. *19th Int. Conf. Electr. Distrib.* 21–24 (1980).

18. Hansen, P. & Watt, A. VLF/LF High-Voltage Design and Testing. *DTIC Doc.* (2003).

19. Xiao, C., Bin, Z. & Huang, W. Z. Analysis for the abnormal growth of bushing dielectric loss in a 500KV transformer. in *China International Conference on Electricity Distribution, CICED* **2014–Decem,** 1574–1577 (2014).

20. Li, Z., Lina, Z., Qingmin, L., Liang, Z. & Chunhui, Y. Electric field computation of ±1000 kv dc wall bushing with consideration of space charge effects. *Int. Trans. Electr. Energy Syst.* **24,** 297–304 (2014).

21. Ning, X. *et al.* Dielectric properties of multi-layer epoxy resinimpregnated crepe paper composites. *IEEE Trans. Dielectr. Electr. Insul.* **22,** 161–168 (2015).

22. Kiiza, R. C., Niasar, M. G., Nikjoo, R., Wang, X. & Edin, H. Change in partial discharge activity as related to degradation level in oil-impregnated paper insulation: Effect of high voltage impulses. *IEEE Trans. Dielectr. Electr. Insul.* **21,** 1243–1250 (2014).

23. Vas, J. V., Venkatesulu, B. & Thomas, M. J. Tracking and erosion resistance of silicone rubber nanocomposites under positive and negative dc voltages. in *Annual Report - Conference on Electrical Insulation and Dielectric Phenomena, CEIDP* (2010). doi:10.1109/CEIDP.2010.5724032

24. Wang, M., Vandermaar, A. J. & Srivastava, K. D. Review of condition assessment of power transformers in service. *IEEE Electrical Insulation Magazine* **18,** 12–25 (2002).

25. Ahmadi-Joneidi, I., Majzoobi, A., Shayegani-Akmal, A., Mohseni, H. & Jadidian, J. Aging

evaluation of silicone rubber insulators using leakage current and flashover voltage analysis. *IEEE Trans. Dielectr. Electr. Insul.* **20,** 212–220 (2013).

26. Kim, H. K. & Shi, F. G. Thickness dependent dielectric strength of a low-permittivity\ndielectric film. *IEEE Trans. Dielectr. Electr. Insul.* **8,** 248–252 (2001).

27. Kim, Y. H. *et al.* Dielectric Characteristics of Solid Insulation Materials With Respect to Surface Roughness. *IEEE Trans. Appl. Supercond.* **25,** 1–4 (2015).

28. Inuishi, Y. & Powers, D. A. Electric breakdown and conduction through mylar films. *J. Appl. Phys.* **28,** 1017–1022 (1957).

29. Du, B. X., Ma, Z. L., Gao, Y. & Han, T. Effect of ambient temperature on electrical treeing characteristics in silicone rubber. *IEEE Trans. Dielectr. Electr. Insul.* **18,** 401–407 (2011).

30. Gonon, P., Sylvestre, A., Teysseyre, J. & Prior, C. Combined effects of humidity and thermal stress on the dielectric properties of epoxy-silica composites. *Mater. Sci. Eng. B* **83,** 158–164 (2001).

31. Rizk, F. A. M. & Rezazada, A. Q. Modeling of altitude effects on AC flashover of polluted high voltage insulators. *IEEE Trans. Power Deliv.* **12,** 810–822 (1997).

32. Bhushan, B. & Jung, Y. C. Natural and biomimetic artificial surfaces for superhydrophobicity, self-cleaning, low adhesion, and drag reduction. *Prog. Mater. Sci.* **56,** 1–108 (2011).

33. Kota, A. K., Kwon, G. & Tuteja, A. The design and applications of superomniphobic surfaces. *NPG Asia Materials* **6,** (2014).

34. Vahabi, H., Wang, W., Davies, S., Mabry, J. M. & Kota, A. K. Coalescence-Induced Self-Propulsion of Droplets on Superomniphobic Surfaces. *ACS Appl. Mater. Interfaces* **9,** 29328–29336 (2017).

35. Wang, W. *et al.* Metamorphic Superomniphobic Surfaces. *Adv. Mater.* **29,** 1700295 (2017).

36. Pendurthi, A. *et al.* Fabrication of Nanostructured Omniphobic and Superomniphobic Surfaces with Inexpensive CO_2 Laser Engraver. *ACS Appl. Mater. Interfaces* **9,** 25656–25661 (2017).

37. Vahabi, H. *et al.* Metallic superhydrophobic surfaces via thermal sensitization. *Appl. Phys. Lett.* **110,** 251602 (2017).

38. Movafaghi, S. *et al.* Hemocompatibility of Superhemophobic Titania Surfaces. *Adv. Healthc. Mater.* **6,** 1600717 (2017).

39. Kota, A. K., Mabry, J. M. & Tuteja, A. Superoleophobic surfaces: design criteria and recent studies. *Surf. Innov.* **1,** 71–83 (2013).

40. Vahabi, H. *et al.* Metallic superhydrophobic surfaces via thermal sensitization. *Appl. Phys. Lett.* **110,** (2017).

41. Bark, D. L. *et al.* Hemodynamic Performance and Thrombogenic Properties of a Superhydrophobic Bileaflet Mechanical Heart Valve. *Ann. Biomed. Eng.* **45,** 452–463 (2017).

42. Wang, W. *et al.* Superhydrophobic Coatings with Edible Materials. *ACS Appl. Mater. Interfaces* **8,** 18664–18668 (2016).

43. Beemer, D. L., Wang, W. & Kota, A. K. Durable gels with ultra-low adhesion to ice. *J. Mater. Chem. A* **4,** 18253–18258 (2016).

44. Butt, H.-J. *et al.* Characterization of super liquid-repellent surfaces. *Curr. Opin. Colloid Interface Sci.* **19,** 343–354 (2014).

45. Young, T. An Essay on the Cohesion of Fluids. *Philos. Trans. R. Soc. London* **95,** 65–87 (1805).

46. Bonn, D., Eggers, J., Indekeu, J. & Meunier, J. Wetting and spreading. *Rev. Mod. Phys.* **81,** 739–805 (2009).

47. Nosonovsky, M. & Bhushan, B. Superhydrophobic surfaces and emerging applications: Non-adhesion, energy, green engineering. *Current Opinion in Colloid and Interface Science* **14,** 270–280 (2009).

48. Furmidge, C. G. L. Studies at phase interfaces i. the sliding of liquid drops on solid surfaces and a theory for spray retention. *j. colloid Sci.* **17,** 309–324 (1962).

49. Wenzel, R. N. Resistance of Solid Surfaces. *Ind. Eng. Chem.* **28,** 988–994 (1936).

50. Cassie, A. B. D. & Baxter, S. Wettability of porous surfaces. *Trans. Faraday Soc.* **40,** 546 (1944).

51. Bittoun, E. & Marmur, A. The Role of Multiscale Roughness in the Lotus Effect: Is It Essential for Super-Hydrophobicity? *Langmuir* **28,** 13933–13942 (2012).

52. Vallet, M., Berge, B. & Vovelle, L. Electrowetting of water and aqueous solutions on poly(ethylene terephthalate) insulating films. *Polymer (Guildf).* **37,** 2465–2470 (1996).

53. Novoselov, K. S. *et al.* Electric field effect in atomically thin carbon films. *Science* **306,** 666–9 (2004).

54. Wang, H., Peng, Z., Zhang, S. & Liu, P. Simulation study on E-field distribution and corona characteristics of composite insulator with water droplets. in *Annual Report - Conference on Electrical Insulation and Dielectric Phenomena, CEIDP* 422–425 (2013). doi:10.1109/CEIDP.2013.6747443

55. Joneidi, I. A., Kamarposhti, M. A., Shayegani Akmal, A. A. & Mohseni, H. Leakage current analysis, FFT calculation and electric field distribution under water droplet on polluted silicon rubber insulator. *Electr. Eng.* **95,** 315–323 (2013).

56. Schultz, T., Pfeiffer, M. & Franck, C. M. Optical investigation methods for determining the impact of rain drops on HVDC corona. *J. Electrostat.* **77,** 13–20 (2015).

57. Frącz, P. Influence Estimation of the Voltage Value on the Measurement Results for the Optical Radiation Generated by Partial Discharges on Bushing Isolator. *Opt. Acoust. Methods Sci. Technol.* **120,** (2011).

58. Que, W. & Sebo, S. Typical cases of electric field and voltage distribution calculations along polymer insulators under various wet surface conditions. *Electr. Insul. Dielectr. ...* 840–843 (2002).

59. Hara, M., Ishibe, S. & Akazaki, M. Corona discharge and electrical charge on water drops dripping from D.C. transmission conductors - an experimental study in laboratory. *J. Electrostat.* **6,** 235–257 (1979).

60. Jiang, X., Yuan, Y., Bi, M., Du, Y. & Ma, J. DC positive discharge performance of rod-plane short air gap under rain conditions. *IEEE Trans. Dielectr. Electr. Insul.* **20,** 104–111 (2013).

61. Reddy, B. S., Kumar, a., Shashikala, a. & Ravishankar, K. V. Electric Field Modelling of Composite High Voltage Insulators. *India Conf. (INDICON), 2009 Annu. IEEE* 3–6 (2009). doi:10.1109/INDCON.2009.5409458

62. Karady, G. *et al.* A mitigation method for dry-band arcing caused deterioration of ADSS fiberoptic cables. in *2000 IEEE Power Engineering Society Winter Meeting. Conference Proceedings (Cat. No.00CH37077)* **4,** 2391–2396 (IEEE).

63. Seog-Hyeon Kim, Cherney, E. A., Hackam, R. & Rutherford, K. G. Chemical changes at the surface of RTV silicone rubber coatings on insulators during dry-band arcing. *IEEE Trans. Dielectr. Electr. Insul.* **1,** 106–123 (1994).

64. Hesamzadeh, M. R., Hosseinzadeh, N. & Wolfs, P. An advanced optimal approach for high voltage AC bushing design. *IEEE Trans. Dielectr. Electr. Insul.* **15,** 461–466 (2008).

65. Movafaghi, S. *et al.* Tunable superomniphobic surfaces for sorting droplets by surface tension. *Lab Chip* **16,** 3204–3209 (2016).

66. Vahabi, H., Wang, W., Movafaghi, S. & Kota, A. K. Free-Standing, Flexible, Superomniphobic Films. *ACS Appl. Mater. Interfaces* **8,** 21962–21967 (2016).

67. Gelest. Gelest. *Silane coupling agents*

68. Kota, A. K., Choi, W. & Tuteja, A. Superomniphobic surfaces: Design and durability. *MRS*

Bull. **38,** 383–390 (2013).

69. Trichel, G. W. The mechanism of the negative point to plane corona near onset. *Phys. Rev.* **54,** 1078–1084 (1938).